ELECTROSTATIC SCREENING BY SELF-CONSISTENT SPACE CHARGE, AND THE ION DYNAMICS IN A TIME-OF-FLIGHT MASS SPECTROMETER

N. A. Inogamov

UDC 533.95+621.738.478

We construct a theory of an inertially dispersed collisionless plasma cloud in an external electric field F_{ex}. The solution of this problem is applied to the calculation of time-of-flight mass spectrometer.

1. INTRODUCTION

The chemical composition of comet dust in the Galileo comet was determined by dust-impact mass analyzer (DIMA) which was placed on board of the cosmic apparatus Vega and Giotto [1-4]. The dust-impact mass analyzer combines a dust accelerator and a time-of-flight mass spectrometer (TFMS) of the type "mass reflectron" [4, 5]. The Van de Graaf and Heidelberge accelerators are used as dust accelerators in the natural modeling [6]. The present work is devoted to a theoretical study of the DIMA device. The study contains a calculation of the steady flow, a perturbation theory I which takes into account the correction associated with a small nonstationarity of the source, and a perturbation theory II which is devoted to the case of multicomponent plasma.

A complete investigation of the operation of the device must relate the output signal $I_c(t)$ (see Fig. 1) to the input parameters μ, β, M, N_0. We shall call this an applied problem as a whole. Its solution includes a systematic solution of a chain of four sections which represent different physical problems; Sec. 3 (inertially dispersed collisionless plasma cloud (PC) in an electric field (EF) is the most difficult. Sec. 1 determines the dispersion kinematics of the dust substance after collision with the anode (see Fig. 1) and the asymptotic form of PC in the velocity space. Section 2 is a plasmachemical problem which relates N_0 to the frozen composition of the plama N. Finally, in Sec. 4, the obtained results are used to determine $I_c(t)$ by calculating the ion optics of TFMS. This work is restricted to the description of the last two sections.

We note that the problem allows the following simplifications of a technical nature. 1. Inductive components are insignificant. 2. Secondary electrons which knock out ions falling into the wires of the accelerating grid can be neglected since, first, the interception coefficient of the grid is small and, second, the ionization-accelerating chamber (IAC) uses low ($\simeq$ 1 kV) voltage. If the metal surface is bombarded by ions with this energy, the electron yield is $\ll 1$. 3. The change of $\phi_a(\dot{\phi}_a = 0)$ can be neglected as a result of the anode discharge by electrons which arrive at the anode from PC. This is because the accelerating grid 1 of IAC is earthed via a capacitor with $C \gg ZeN/\phi_a$ which is connected in parallel to the capacitance between the grid and the anode (see Fig. 1).

2. ELECTROSTATIC SELF-CONSISTENT FIELD OF THE SPACE CHARGE AND THE ION OPTICS OF THE TIME-OF-FLIGHT MASS SPECTROMETER

When a dust grain hits the anode, a dispersing plasma cloud is formed (Fig. 1). An analysis makes it possible to isolate five characteristic stages: 1) the establishment of inertial regime of dust plasma dispersal; 2) freezing of ionization; 3) transition to the regime of collisionless flow; 4) initial stage of the interaction of the EF with the dynamics of PC which is considerably affected by the space charge; 5) final stage of the EF interaction in which the electrostatic self-consistent field of the space charge (ESCFSC) does not play a role.

L. D. Landau Institute of Theoretical Physics, Academy of Sciences of the USSR, Moscow.
Translated from Inzhenerno-Fizicheskii Zhurnal, Vol. 52, No. 4, pp. 553-562, April, 1987. Original article submitted September 17, 1985.

 0022-0841/87/5204-0396$12.50

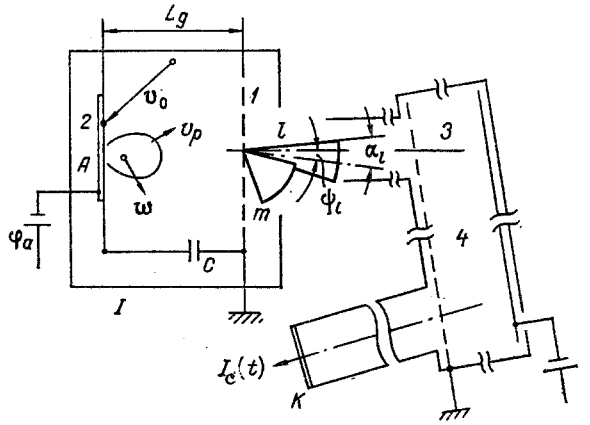

Fig. 1

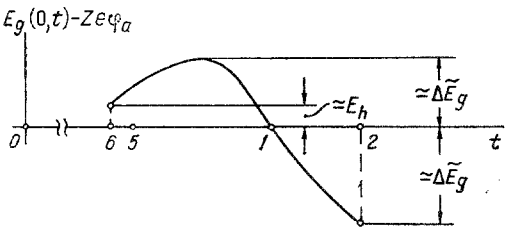

Fig. 2

Fig. 1. Diagram of the DIMA device. I) IAC; 1) ion extracting grid; 2) point of impact of the dust grain; 3) axis of the entrance tube; 4) reflector; K) collector; A) plasma generating element (anode).

Fig. 2. Dependence $E_g(0, t)$ in the range II of values N: 1) $t_1 \simeq t_*$; 2) $t_2 \simeq t_*$, $t_2 > t_1$; 5) at time $2L_g/v_{g.0}$; the time segment between moments 5 and 6 is $\simeq t_n = R_n/v_h$.

We discuss briefly the expansion kinetics. The gas dynamic conditions under oblique impact are complicated. In particular, as a result of the presence of a glide plane which is unstable according to Kelvin and Helmholtz, a small part of the dust substance is mixed with the anode. Particularly complex is the flow for $\mu > 1$ when the penetration depth of the dust into the anode is long. In this case, the anode plasma leads the dust plasma. We confine ourselves to the case $\mu < 1$. The experiments [1] use platinum or silver anodes. Then $\mu = 0.2$-0.3. For $\mu < 1$, the anode plasma disperses slowly, lags behind the dust plasma and does not affect the interaction of the EF F_{ex} with PC from the dust substance.

For $\mu < 1$, a simplified model of the dispersal is useful. In th is model, the motion of PC is characterized by the velocities w and $v_h = \sqrt{\frac{2E_h}{m_i}}$, where w is the drift velocity of PC as a whole, and v_h is the expansion velocity. Everywhere in the present work, with the exception of the concluding part of Sec. 3, we consider the case $w_\perp < v_h$ when the solid angle subtended by the collector as "seen" from the accelerating grid 1 of IAC (see Fig. 1) is inside a cone which contains the velocity vectors of the ions which escape beyond this grid.

Concerning the frozen composition of the plasma, it follows from [7, 8] that $N \simeq N_0$, $Z \simeq 1$.

Following these remarks concerning stages 1 and 2, we turn to the ion dynamics in EF.

To simplify the formulae, we introduce normalization with respect to N_c and the notation

$$\hat{N} = \frac{N}{N_c}, \quad N_c = \frac{\varphi_a L_g}{Ze}, \quad \varepsilon = \frac{E_h}{Ze\varphi_a}, \quad \varepsilon_1 = \frac{L_g}{2L_T}.$$

There are important scales R_n and R_d, where $R_n = E_h/ZeF_{ex} = \varepsilon L_g$; $R_d = \sqrt{ZeN/F_{ex}}$. Depending on their ratio

$$R_n/R_d = \sqrt{N_1/N}, \quad N_1 = E_h^2/Z^3e^3F_{ex}, \quad \hat{N}_1 = \varepsilon^2$$

the following cases are possible:

$$R_n \gg R_d, \quad N \ll N_1; \tag{2.1}$$

$$R_n \ll R_d, \quad N \gg N_1. \tag{2.2}$$

The space charge is important in the case (2.2) and unimportant for (2.1). In conditions (2.2), we have $R_2 \gg R_n$. During plasma dispersal up to the radius $R \simeq R_2$, the following condition then holds:

$$t_Q/t_h = \sqrt{R_n/R} \ll 1. \tag{2.3}$$

Consequently, ESCFSC varies slowly with time compared with t_Q. The smallness of the nonstationarity parameter (2.3) indicates the inapplicability of the steady-state approximation which is given by the zero-order term in the expansion of the exact solution with respect to the parameter (2.3).

It follows from the study of the flow in the steady-state approximation that, in conditions (2.2), the following relation holds:

$$R_2 \simeq R_* = (Zem_i N^2 v_h^2 / 2F_{ex}^3)^{1/5}. \tag{2.4}$$

In the case (2.1) we have $R_2 \simeq R_d \sim N^{1/2}$.

Relation (2.4) is suitable for

$$R_* \ll L_g,\ N \ll N_2,\ N_2 = N_1/\varepsilon^{2,5}. \tag{2.5}$$

For $N > N_2$, it is necessary to take into account the compression of the accelerating segment of IAC by the grid 1 (see Fig. 1). In the present work we restrict ourselves to the study of the case (2.5) which is sufficient for the chosen application.

For the DIMA device we have $v_0 = 78$ km/sec, $v_h \simeq 10$ km/sec, $F_{ex} \simeq 1$ kV/cm, $R_0 = 0.1$-1 μm, $L_g \simeq 1$ cm. For these values of the parameters

$$\varepsilon = R_n/L_g \ll 1. \tag{2.6}$$

Under the condition (2.6) we have the following classification of the dust with respect to the number N: I) gasdynamic range (2.1) of small dust grains; II) intermediate range $N_1 \ll N \ll N_2$, and the range III of large grains $N > N_2$. The smallness of the parameter ε which is due to the smallness of v_h broadens the boundaries of the range II: $N_2/N_1 = \varepsilon^{-5/2} \gg 1$.

In ranges I and II, the flow has a single-flow character, and will be described by the functions $n_i(r, t)$, $v(r, t)$. We consider the axisymmetric case. In place of $v(r, t)$, we use the functions

$$E(r, z, t),\quad \theta(r, z, t),\quad E_g'(r, t) \equiv E(r, z_g, t),\quad \theta_g(r, t), \tag{2.7}$$

where r and z are the cylindrical coordinates, θ is the angle between v and the z axis, $E = m_i v^2/2$; $z = z_g$ is the plane of the grid 1 (see Fig. 1).

We shall not, for the moment, consider the angular distribution and permeability. We find $(\Delta t)_v$ for the case of small collector: $\Omega_c \to 0$, where

$$\Omega_c = \pi\alpha_c^2;\ \alpha_c = r_c/2L_T; \tag{2.8}$$

and Ω_c is the solid angle subtended by the collector as "seen" from the exit of IAC, r_c is the collector radius, and the coefficient 2 is determined by the motion of ions in the reflector.

We calculate first the function $E_g(0, t)$ which characterizes the energy distribution of ions. In region I, this does not present difficulties. We introduce the notation $\Delta E_g = \Delta E_g(t) = E_g(0, t) - Ze\phi_a$. We have

$$\Delta E_g(t) = E_h f(t), \tag{2.9}$$

where $f(t)$: $f(t) > 0$; and the change of $f(t)$ during the time $\simeq (\Delta t)_t$ during which the bulk of ions intersects the grid of IAC is $\simeq 1$.

We denote by $\Delta\tilde{v}_g$ the scatter of velocity component parallel to the axis of the entrance tube of TFMS (see Fig. 1, the axis of the entrance tube is perpendicular to the accelerating grid of IAC) for the bulk of ions at the exit from IAC. In TFMS with a single ion reflector, there is a double focusing of the ions with respect to energy: in IAC,

$$\frac{\Delta\tilde{v}_g}{v_{g,0}} \simeq \frac{1}{2}\,\frac{\Delta\tilde{E}_g}{Ze\varphi_a},\ v_{g,0} = \sqrt{\frac{2Ze\varphi_a}{m_i}} \tag{2.10}$$

and in the reflector,

$$(\Delta t)_v/t_T \simeq (1/2)(\Delta\tilde{v}_g/v_{g,0})^2, \tag{2.11}$$

where $\Delta\tilde{E}_g$ is the energy scatter of the bulk of ions at the exit from IAC, and t_T is the transit time in TFMS.

It follows from Eqs. (2.10), (2.11), and (2.9) that in the region I,

$$(\Delta t)_v/t_T \simeq \varepsilon^2. \tag{2.12}$$

We now calculate $E_g(0, t)$ and $(\Delta t)_v$ associated with the width of the energy distribution, in the range II. For $t < t_2$, as long as PC is not completely depleted of electrons, there is an electrically neutral region filled with electrons which is screened by the space charge from the external EF F_{ex}. At the boundary of this region, the electron density vanishes discontinuously. The ions which are outside this region will be called "stripped." As the electrons are removed from PC, the surface S moves along the electrically neutral plasma, and new parts of ions are stripped. The surface S will be called the electroablation front (EAF).

In the case under consideration, PC is in contact with the anode (see Fig. 1). The electroablation front is an equipotential surface with potential equal to ϕ_a. As a result, with accuracy up to $\Delta\tilde{E}_g \ll Ze\phi_a$, there is an isoenergetic distribution at the exit from IAC.

It is found that the main contribution to $(\Delta t)_v$ in region II is associated with the time variation of ESCFSC which is caused by the displacement of EAF. There are two reasons which lead to the displacement of EAF: convective drift and the proper electroablation drag of the ions. The convective drift increases the volume of the region encompassed by EAF, and the electroablation tends to reduce this volume. Up to some time $t_1 \simeq t* = R*/v_h$ (everywhere in this work, the time is measured from the impact time), EAF expands as result of the fact that the convective velocities exceed the velocity of electroablation. It can be shown that the expanding surface of EAF pushes the ions. This push leads to the fact that an ion at the grid has energy $E_g > Ze\phi_a + E_h$ (Fig. 2).

From the time t_1, the volume of the region bounded by EAF begins to contract. This leads to "deceleration" of ions, and their energy is reduced: $E_g < Ze\phi_a + E_h$. For $t = t_2 \simeq t*$, the region bounded by EAF reduces to a point.

We note one fact. It is not difficult to show that the segment of ion trajectory which is enclosed in the region of localization of ESCFSC contains two parts: region of additional acceleration (in comparison with the rigorous steady state), and the region of deceleration. If EAF expands, the deceleration occurs first, and is followed by acceleration. The deceleration is associated with the fact that, during the expansion of EAF, the ion remains longer in a region with a weaker accelerating field since in EAF, the EF intensity $F = 0$. As a result, it is found that the additional acceleration on the second segment is more pronounced than the deceleration on the first segment. The sign of the total effect is always determined by the second segment. This can easily be shown by using the energy integral in a field with a slowly time varying relief of the potential surface.

During the contraction of EAF, an additional acceleration initially follows, and then deceleration.

A characteristic scale of change of the intensity of ESCFSC δF during a time interval $\simeq t_Q$ and the dependence $\Delta E_g(t)$ are as follows:

$$\delta F \simeq F_{ex} = \frac{t_Q(R)}{t_h(R)}, \quad \Delta E_g(t_4) = Ze\int_{t_3}^{t_4} dt\left((\delta F(r(t),\ t)\frac{dr(t)}{dt}\right).$$

Hence, after transformations

$$\Delta E_g(t_4) \simeq ZeR(t_3)(\delta F) \simeq ZeF_{ex}v_h t_Q(R(t_3)), \tag{2.13}$$

where t_3, t_4 are the moments when the ion intersects EAF and the accelerating net, respectively, $t_3 = t_3(t_4)$; $r(t)$ is the trajectory of an ion which, at the moment t_4, intersects the accelerating net in point $r = 0$. In the derivation of (2.13) is was assumed that the modulus of velocity of EAF displacement is always, in the order of magnitude, equal to v_h. Indeed, for $t < t_1$, this is obvious. For $t_1 < t < t_2$, the modulus of the velocity of EAF motion $\simeq v_a$. But for $t \simeq t*$ (and the quantities t_1 and t_2 are both $\simeq t*$) as can be shown, for v_a, we have $v_a \simeq v_h$. Therefore, (2.13) is applicable for $0 < t < t_2$.

In accordance with (2.13) on the upward segment, the dependence $\Delta E_g(t)$ (see Fig. 2) is given by the formula

$$\Delta E_g(t) = c\sqrt{\left(t - \frac{2L_g}{v_{g,0}}\right)E_h v_h ZeF_{ex}}, \quad c \simeq 1. \tag{2.14}$$

Indeed, from (2.13) we have $\Delta E_g(t_4) = c\sqrt{E_h v_h ZeF_{ex} t_3}$. It is not difficult to see that $t_4 - t_3 = c_2 t_Q(R(t_3)) + 2L_g/v_{g,0}$ where the constant $|c_2| \simeq 1$. For $t_3 \gg t_Q(R(t_3))$ (one must also have $R(t_3) \gg R_n$) we have $t_4 \simeq 2L_g/v_{g,0} + t_3$, and hence follows (2.14).

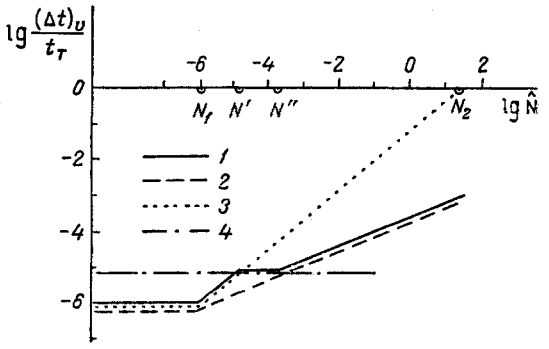

Fig. 3

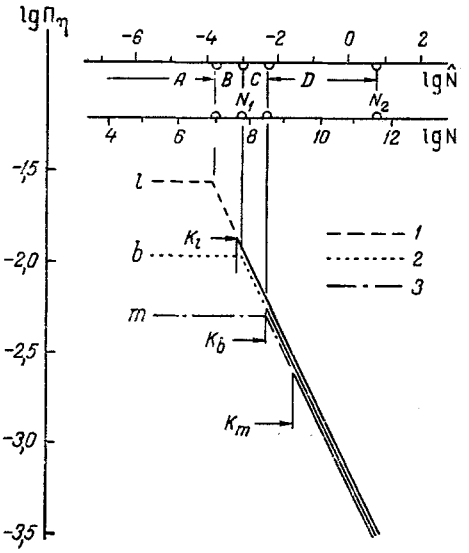

Fig. 4

Fig. 3. Dependence $(\Delta t)_v/t_T$ on N in the case $\alpha_h < \alpha_c$ for carbon (v_h = 10 km/sec, ϕ_a = 3 kV, Z = 2, α_c = 3°): 1) the resulting dependence $(\Delta t)_v/t_T$; 2) the dependence $(\Delta t)_v/t_T$, where $(\Delta t)_v$ is determined by the distribution E_g; 3) $(\Delta t)_v/t_T$, where $(\Delta t)_v$ is determined by the distribution θ_g for $\alpha_c = \pi/2$. The straight line 4 corresponds to the value on the ordinate axis α_c^4.

Fig. 4. Dependences $\Pi_\eta(\hat{N})$ for α_c = 1° (carbon chondrite): ions C^+, Si^+, Fe^+ are denoted by indices ℓ, b and m, respectively; ϕ_a = 3 kV, L_g = 3 cm, $w_\perp$ = 35 km/sec, v_h = 25 km/sec, Z = 1; the lines 1, 2, and 3 show the dependences $\Pi_\eta(\hat{N})$ which hold for $w_\perp < v_h$.

We note that the quantity $t - 2L_g/v_{g,0}$ in (2.14) changes, for $N \gg N_1$, in a logarithmically wide interval of values (from $\simeq t_n = R_n/v_h$ to $\simeq t* \gg t_n$). For $N \to N_2$ $t* \to L_g/v_h$.

From (2.13) we find $\Delta\tilde{E}_g \simeq \Delta E_g(t_4)$, here t_4: $t_3 = t_3(t_4) = t*$. From this condition and from Eqs. (2.10), (2.11) and (2.14) we obtain, after transformations, the required expression for the line width caused by the energy scatter at the exit from IAC:

$$(\Delta t)_v/t_T = c_1\varepsilon^{1,2}\hat{N}^{0,4},\ c_1 \simeq 1. \tag{2.15}$$

Above we solved the difficult problem for the energy distribution of ions and the associated quantity $(\Delta t)_v$. The total width of the mass-spectrometric line is equal to $\Delta t = (\Delta t)_t + (\Delta t)_v$, where $(\Delta t)_v$ is given by (2.15). Concerning $(\Delta t)_t$, in the range II we have $(\Delta t)_t \simeq t*$. Thus, the problem of the line width has been exhausted.

We now turn to the angular distribution of ions. The instantaneous velocity diagram at the exit from IAC is obtained by variation of r on the $z = z_g$ plane (see (2.7)). The velocity diagram is a cone with the opening angle 2α.

It is not difficult to see that in the range I,

$$\alpha \simeq \alpha_h,\quad \alpha_h = v_h/v_{g,0} = \sqrt{\varepsilon}. \tag{2.16}$$

To simplify the calculations we restrict ourselves to accuracy $\tan\alpha \approx \sin\alpha \approx \alpha$.

In the range II, the angle α is determined by scattering and acceleration of ions in the region of localization of ESCFSC. As a result of this interaction with ESCFSC, the velocity component of the bulk of ions which is transverse to F_{ex} reaches the values $\simeq v_Q(R*)$. Accordingly, we obtain for α the expression:

$$\alpha \simeq v_Q(R_*)/v_{g,0} = \varepsilon^{0,1}\hat{N}^{0,2}. \tag{2.17}$$

For $R* \simeq L_g$, we have $\alpha \simeq \pi/2$.

We investigate the effect of the receiving aperture of TFMS which is characterized by the angles α_c, Ω_c. The quantities α and $(\Delta t)_t$ are independent of α_c, and this is why the functions $(\Delta t)_v$ and N_c/N may depend on α_c.

There are two possible cases: $\alpha_c < \alpha_h$ and $\alpha_h < \alpha_c$. We consider first the first case which is simpler. It can be shown that the distribution of $\theta_g(r, t)$ is then insignificant

in the determination of $(\Delta t)_v$. The quantity $(\Delta t)_v/t_T$ is given by formulas (2.12) and (2.14) in the ranges I and II, respectively. For N_c/N we have

$$N_c/N \simeq (\alpha_c/\alpha)^2, \tag{2.18}$$

where α is given, in the ranges I and II, by formulae (2.16) and (2.17), respectively.

We consider the case of wide collector and small velocities v_h:

$$\alpha_h < \alpha_c. \tag{2.19}$$

The contribution of the angular distribution θ_g to $(\Delta t)_v$ is obtained by projection of the isoenergetic distribution ($\Delta E_g \ll Ze\phi_a$) onto the axis of the entrance tube of TFMS.

From (2.16) and (2.19) we have in region I for the scatter $\Delta\tilde{v}_g$ caused by the distribution of θ_g:

$$\Delta\tilde{v}_g/v_{g,0} \simeq \alpha_h^2/2. \tag{2.20}$$

From (2.12), (2.10) and (2.11) we obtain in region I for the resolving power $(\Delta t)_v/t_T$ associated with θ_g:

$$(\Delta t)_v/t_T \simeq \alpha_h^4/8. \tag{2.21}$$

It is seen from the comparison of Eqs. (2.21), (2.12) and using (2.16) that in region I, the contributions to $(\Delta t)_v$ associated with the E_g and θ_g distributions are of the same order of magnitude under the condition (2.19) (see Fig. 3).

The dependence of $(\Delta t)_v/t_T$ on N in conditions (2.19) is shown in Fig. 3. The above formulae determine the required quantities with accuracy up to a numerical coefficient $\simeq 1$. In the construction of the graphs, all these coefficients will be set equal to 1. This refers also to Fig. 4.

For $N_1 < N < N'$, the ratio $(\Delta t)_v/t_T$ is due to the angular distribution θ_g and is equal to

$$(\Delta t)_v/t_T \simeq \alpha^4 = c\varepsilon^{0,4}\hat{N}^{0,8},\ c \simeq 1.$$

For $N'' < N < N_2$, the quantity $(\Delta t)_v/t_T$ is determined by the energy distribution E_g and is given by (2.15).

From the equation $\alpha(N') = \alpha_c$ where $\alpha(N)$ is given by (2.17), we obtain an expression for $N' = \alpha_c^5\sqrt{\varepsilon}$, and from the equation $\varepsilon^{1,2}\hat{N}^{0,4} = \alpha_c^4$ (these are the conditions for the intersection of the N dependence of $(\Delta t)_v/t_T$ given by (2.15) and the straight line $(\Delta t)_v/t_T = \alpha_c^4$, see Fig. 3) follows a formula for $\hat{N}'' = \alpha_c^{10}/\varepsilon^3$. We note that the condition $N'' > N'$ is equivalent to (2.19).

The dependence of the permeability N_c/N on N in the case (2.19) has the form $N_c/N = 1$ for $N < N'$ (here $\alpha < \alpha_c$); for $N' < N < N_2$ (here $\alpha > \alpha_c$), the quantity N_c/N is given by formula (2.18).

3. THE CASE OF MULTICOMPONENT PLASMA

We consider, within the framework of perturbation theory, a mixture of light (ℓ), base (b), and heavy (m) ions. We restrict ourselves to the case $Z_\ell = Z_b = Z_m = Z$. We introduce the index η which runs through the values ℓ, b, and m, and we also introduce the following notation:

$$\varkappa_\eta = \frac{m_\eta}{m_b},\ \varepsilon = \frac{R_{nb}}{L_g},\ R_{n\eta} = \varkappa_\eta R_{nb},\ R_{nb} = \frac{E_{hb}}{ZeF_{ex}},$$

$$E_{hb} = \frac{m_b v_h^2}{2},\ R_d = \sqrt{\frac{ZeN}{F_{ex}}},\ N = N_l + N_b + N_m,\ \varepsilon_1 = \frac{L_g}{2L_T}, \tag{3.1}$$

$$P_{v\eta} = \frac{t_{T\eta}}{(\Delta t)_{v\eta}},\ P_{t\eta} = \frac{t_{T\eta}}{(\Delta t)_{t\eta}},\ \Pi_\eta = \frac{N_{c\eta}}{N_\eta},$$

where $t_{T\eta}$, $N_{c\eta}$ are the transit time of TFMS and the number of ions of type η captured by the collector, $(\Delta t)_{v\eta}$, $(\Delta t)_{t\eta}$ are the width of the η lines in the mass spectrum caused by the velocity scatter in a group of ions arriving at the collector, and by the finite time of intersection of the bulk of η ions of the accelerating grid of IAC, respectively.

The limits of applicability of the perturbation theory are as follows: $N_l < cN_b$, $c \simeq 1$; $N_m \ll N_b$. It is important to emphasize that there can be many l ions and, consequently, the theory describes arbitrary mixtures.

It is found that there are 4 subregions of values of N which will be denoted by A, B, C, and D (see Fig. 4). Below, for each of these subregions, we give the boundaries, structure of flow, and the formulas for α and for the resolving power $P_{v\eta}$, $P_{t\eta}$. The permeability coefficients $\Pi_\eta(\hat{N})$ are shown in Fig. 4.

The angle between the axis of the cone containing the ion vectors which pass the accelerating grid of IAC (see Fig. 1) and the normal to the grid is equal to

$$\psi_\eta = \frac{w_\perp}{v_{g\eta}} = \sqrt{\varkappa_\eta}\,\psi_b,\ v_{g\eta} = \sqrt{\frac{2Ze\varphi_a}{m_\eta}}. \tag{3.2}$$

Under the condition $w_\perp < v_h$ ($\psi_\eta < \alpha_\eta$, respectively for all N) supplemented by the condition $\alpha_\eta > \alpha_c$, the quantity Π_η is related to α_η by the simple formula $\Pi_\eta = \alpha_c^2/\alpha_\eta^2$. Therefore, the expressions for Π_η are not given. For $\alpha_\eta < \alpha_c$ and $w_\perp < v_h$, we have $\Pi_\eta(\hat{N}) \equiv 1$.

We consider the subregion A: $\hat{N} < \varkappa_l^2\varepsilon^2$. The sequence of stages during the dispersal of PC is as follows (is it convenient to deal with R rather than t, ($R = v_h t$) for $R \ll R_d$ the stripped η ions form a thin layer at the periphery of PC. For $R \simeq R_d$, PC is completely depleted of electrons. the freed electrons are deposited at the anode. For $R \simeq R_{nl}$, R_{nb}, R_{nm}, it is first the l ions, then the b ions and finally the m ions which are accelerated. All three clouds (l, b, and m) have a spherical form. The calculation gives

$$P_{v\eta} \simeq (\varkappa_\eta\varepsilon)^{-2},\ P_{t\eta} \simeq (\varepsilon_1\sqrt{\varkappa_\eta\varepsilon})^{-1},\ \alpha_\eta \simeq \sqrt{\varkappa_\eta\varepsilon}. \tag{3.3}$$

We turn to subregion B: $\varkappa_l^2\varepsilon^2 < \hat{N} < \varepsilon^2$. For $R < R_{nl}$, the stripped ions form a thin layer at the periphery of PC. For $R \simeq R_d > R_{nl}$, the PC is stripped and the l ions are accelerated. The cloud of l ions is elongated into a beam along F_{ex}. Subsequently, for $R \simeq R_{nb}$, R_{nm}, the b ions are accelerated first, and then the m ions. The clouds of the b and m ions have a spherical shape. The calculation gives

$$P_{vl} \simeq (\varkappa_l\varepsilon\sqrt{\hat{N}})^{-1},\ P_{tl} \simeq \frac{1}{\varepsilon_1}\sqrt{\frac{\varkappa_l\varepsilon}{\hat{N}}},\ \alpha \simeq \hat{N}^{1/4}. \tag{3.4}$$

Analogous quantities for the b and m ions in subregion B are given by Eqs. (3.3).

In subregion C ($\varepsilon^2 < \hat{N} < \varkappa_m^{5/2}\varepsilon^2$) for $R \simeq R^*_b = \varepsilon^{0.2}\hat{N}^{0.4}L_g$, the PC is stripped and the l and b ions (whose clouds form elongated beams) are accelerated. The cloud of m ions has a spherical shape. The calculation gives

$$\begin{gathered} P_{vl} \simeq (\varkappa_l\varepsilon^{1,2}\hat{N}^{0,4})^{-1},\ P_{tl} \simeq \frac{\varepsilon^{0,3}\sqrt{\varkappa_l}}{\varepsilon_1\hat{N}^{0,4}},\ \alpha_l \simeq \varepsilon^{0,1}\hat{N}^{0,2}, \\ P_{vb} \simeq (\varepsilon^{1,2}\hat{N}^{0,4})^{-1},\ P_{tb} \simeq \frac{\varepsilon^{0,3}}{\varepsilon_1\hat{N}^{0,4}},\ \alpha_b \simeq \alpha_l. \end{gathered} \tag{3.5}$$

Analogous quantities for the m ions in subregion C are given by (3.3).

Finally, we turn to subregion D: $\varkappa_m^{5/2}\varepsilon^2 < \hat{N} < \varepsilon^{-1/2}$. For $R \simeq R^*_b$, there is a stripping of PC and the acceleration of the l, b, and m ions. Their clouds have the form of elongated beams. The calculation gives

$$P_{vm} \simeq (\varkappa_m\varepsilon^{1,2}\hat{N}^{0,4})^{-1},\ P_{tm} \simeq \frac{\varepsilon^{0,3}\sqrt{\varkappa_m}}{\varepsilon_1\hat{N}^{0,4}},\ \alpha_m \simeq \varepsilon^{0,1}\hat{N}^{0,2}. \tag{3.6}$$

The expressions for the analogous quantities for the l and b ions in subregion D are the same as in subregion C, and are given by (3.5).

An analysis of (3.3)-(3.6) shows an interesting fact. It is found that

$$P_{t\eta}/P_{v\eta} = (\varkappa_\eta\varepsilon)^{3/2}/\varepsilon_1 \tag{3.7}$$

which is independent of N for $N < N_2$. This relationship, which is specific for TFMS with a single ion reflector, makes it possible to choose optimally the parameters of TFMS for the entire interval of values of N. In the optimal variant $P_{t\eta} = P_{v\eta}$ for a chosen η ion.

In conclusion of this section we consider the case $w_\perp > v_h$. For $0 < N < K_\eta$, the condition $\psi_\eta - \alpha_\eta > \alpha_c$ holds and the corresponding η ions do not reach the collector (see Figs. 1 and 4, cones l and m).

We restrict ourselves to the case when $\alpha_c \ll \alpha_\eta$ and the distribution θ_g has a sharp edge: $\partial N/\partial\Omega$ = const if v is inside the cone, and $\partial N/\partial\Omega = 0$ if v is outside the cone. Then, for $N < K_\eta$, we have $\psi_\eta > \alpha_\eta$, and, consequently, $\Pi_\eta(\hat{N}) = 0$, and for $N > K_\eta$ $\Pi_\eta(\hat{N}) = \alpha_c^2/\alpha_\eta^2$, where $\alpha_\eta(\hat{N})$ is given by Eqs. (3.4)-(3.6) depending on N (see Fig. 4). If one or several of these conditions are violated, transition regions occur near the values $N = K_\eta$ in which $\Pi_\eta(\hat{N})$ varies from 0 to α_c^2/α_η^2.

We calculate the value of K_η which is a root of the equation $\alpha_\eta(\hat{K}_\eta) = \psi_\eta$. Substituting Eqs. (3.2) and (3.4)-(3.6) into this equation, we find $K_\eta \simeq \kappa_\eta^{2.5}\psi_b^5/\sqrt{\varepsilon}$ for $\psi_b > \sqrt{\varepsilon/\kappa_\ell}$ ($w_\perp > v_h/\sqrt{\kappa_\ell}$), where $\psi_b = w_\perp/v_{gb}$. For $\sqrt{\varepsilon} < \psi_b > \sqrt{\varepsilon/\kappa_\ell}$ ($v_h \leq w_\perp < v_h\sqrt{\kappa_\ell}$), formulas for K_b and K_m are conserved, and the formula for K_ℓ takes the form $\hat{K}_\ell \simeq \kappa_\ell^2\psi_b^4$.

NOTATION

$I_c(t)$, ion current at collector of the DIMA device (see Fig. 1) (everywhere, the subscript c denotes quantities which refer to the collector); $\mu = \rho_d/\rho_a$; ρ_d, ρ_a, initial densities of the dust and anode substances, respectively; β, angle between the vector v_0 and the anode surface; v_0, initial velocity of a dust grain (see Fig. 1); M and R_0, mass and the initial radius of a dust grain, respectively; N_0, elemental chemical composition of the dust substance; N, frozen composition of the dust plasma; N, total number of frozen ions in PC; Z is the charge of the frozen ions; $\phi_a = F_{ex}L_g$, potential of the anode in IAC; L_g, anode-grid separation (see Fig. 1); e, electron charge; w, center of mass velocity of PC composed from the dust substance; $w_\perp$, $w_\parallel$, w components perpendicular and parallel to F_{ex}; v_h is the expansion velocity of PC; $E_h = m_i v_h^2/2$; m_i, ion mass; L_T, total length of the tubes of TFMS; t_T, transit time of TFMS; $R = R(t) = v_h t$, instantaneous size of PC; t_2, moment when PC is completely depleted of electrons (the time is measured from the impact); $R_2 = v_h t_2$; $t_Q = R/v_Q(R)$, transit time of an ion through the localization region whose dimension is, in the order of magnitude, always equal to R; $v_Q(R) = \sqrt{2ZeF_{ex}R/m_i}$; $t_h = R/v_h$, time scale during which the field intensity of the space-charge changes by an order of magnitude; Δt, width of the mass-spectrometric line; $(\Delta t)_v$, broadening due to the scatter of the axial velocity component (we note that $(\Delta t)_v \propto t_T \propto L_T$); $(\Delta t)_t$ is the broadening due to a finite duration of operation of the ion source at the entrance to TFMS (of course, this broadening is independent of L_T).

LITERATURE CITED

1. R. Z. Sagdeev, S. I. Anisimov, S. E. Zhitenev, et al., Dokl. Akad. Nauk SSSR, 279, 613 (1984).
2. B. Jost, B. Schueler, and F. R. Krueger, Z. Naturforsch., 37a, 18 (1982).
3. W. Knabe and F. R. Krueger, Z. Naturforsch., 37a, 1335 (1982).
4. G. V. Lebedev and R. S. Churaev, "Ion-optical calculation of time-of-flight mass spectrometer," Preprint of IKI AN SSSR No. 750, Moscow (1982).
5. V. I. Karataev, B. A. Mamyrin, and D. B. Shmikk, Zh. Tekh. Fiz., 41, 1498 (1971).
6. H. Fichtig, H. Grun, and J. Kissel, in: Cosmic Dust (J. A. M. McDonnel, ed.), New York (1978), pp. 607-616.
7. S. Drapatz and K. W. Michel, Z. Naturforsch., 29a, 870 (1974).
8. Yu. B. Malama, "The ionization phenomenon under very-high-velocity impact," Preprint IKI AN SSSR No. 725, Moscow (1982).